ACS Catalysis

Research Article

pubs.acs.org/acscatalysis

Mechanistic Studies of Oxygen Reduction by Hydrogen on PdAg(110)

Carrie A. Farberow,[†] Andres Godinez-Garcia,[‡] Guowen Peng,[†] Juan Francisco Perez-Robles,[‡] Omar Solorza-Feria,[§] and Manos Mavrikakis*[,†]

[†]Department of Chemical and Biological Engineering, University of Wisconsin-Madison, Madison, Wisconsin 53706, United States
[‡]Depto. Materiales, CINVESTAV-IPN, Lib. Norponiente 2000 Fracc. Real de Juriquilla, 76230 Querétaro, Qro, México
[§]Depto. Química, CINVESTAV-IPN, Av. IPN 2508 A.P. 14-740, 07360 México, D.F., México

ABSTRACT: First principles electronic structure calculations based on periodic, self-consistent density functional theory (DFT-GGA) were utilized to study the mechanism of the vapor phase reaction between hydrogen and oxygen on the PdAg(110) alloy surface. The hydrogen−oxygen reaction is an important reaction in the direct synthesis of hydrogen peroxide (H_2O_2) and at the cathode in proton exchange membrane fuel cells (PEMFCs). Our results demonstrate that the minimum energy path involves the initial formation of a peroxyl (OOH) intermediate followed by O−O bond scission, consistent with the minimum energy path shown on the (111) facet of monometallic Pd and Ag surfaces. The lower activation energy barrier for O−O bond scission in OOH versus hydrogenation of OOH to form HOOH, and the low barrier for HOOH decomposition, suggest that PdAg(110) may not be an effective catalyst for the direct synthesis of H_2O_2. The detailed thermochemistry and activation energy barriers of important elementary steps and intermediates in oxygen reduction by hydrogen on PdAg(110) are compared and contrasted with the analogous results recently reported for Pd(111) and Ag(111). Based on the potential energy surfaces, Ag(111) is tentatively predicted to be more selective toward H_2O_2 production than PdAg(110) and Pd(111). The calculated d-band center of the Pd and Ag surface atoms in PdAg(110) reveals that alloying Pd and Ag increases the reactivity of the Ag atoms more than that of the Pd atoms, compared to the respective monometallic close-packed (111) surfaces, and that Ag atoms in PdAg(110) are more reactive than Ag atoms at the step-edge of Ag(211). Still, the overall similarity between the energetics on PdAg(110) and Pd(111) is demonstrated. The Pd surface atoms in PdAg(110) behave as 1D arrays of more active surface sites and essentially dominate surface chemistry.

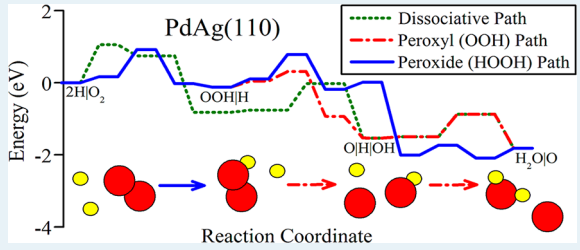

KEYWORDS: *catalysis, oxygen reduction reaction, hydrogen peroxide, PdAg, density functional theory*

1. INTRODUCTION

Dating back to the introduction of the term "catalysis," the direct reaction between hydrogen and oxygen on catalytic surfaces has been an intensely studied research topic.[1,2] Recent work is motivated by the important role of the oxygen reduction reaction (ORR) taking place at the cathode of proton exchange membrane fuel cells (PEMFCs)[3−6] and in the direct synthesis of hydrogen peroxide (H_2O_2).[7−9] The current method for H_2O_2 production is via the anthraquinone autoxidation process, which circumvents explosive H_2−O_2 mixtures. However, this process has several drawbacks which contribute to its high capital and operating costs, including expensive periodic replacement of the quinine component, use of a complex and toxic solvent system, and energy intensive separation steps.[7,8]

An alternative method for hydrogen peroxide production is the direct synthesis of H_2O_2 from H_2 and O_2, which is a thermodynamically favorable reaction:

$$H_2 + O_2 \rightarrow H_2O_{2(l)} \quad \Delta G^0_{298K} = -120.4 \text{ kJ/mol} \tag{1}$$

Yet, the nonselective oxidation of H_2 to water is thermodynamically even more driven:

$$H_2 + \frac{1}{2}O_2 \rightarrow H_2O_{(l)} \quad \Delta G^0_{298K} = -237.2 \text{ kJ/mol} \tag{2}$$

H_2O_2 decomposition (3) and H_2O_2 hydrogenation (4) are also thermodynamically favorable but undesirable side-reactions:

$$H_2O_{2(l)} \rightarrow H_2O_{(l)} + \frac{1}{2}O_2 \quad \Delta G^0_{298K} = -116.8 \text{ kJ/mol} \tag{3}$$

$$H_2O_{2(l)} + H_2 \rightarrow 2H_2O_{(l)} \quad \Delta G^0_{298K} = -354.0 \text{ kJ/mol} \tag{4}$$

For direct H_2O_2 synthesis to be a feasible alternative to the anthraquinone process, identification of a direct synthesis catalyst that selectively catalyzes reaction 1 is necessary.

Received: April 10, 2013
Revised: May 27, 2013
Published: June 3, 2013

   dx.doi.org/10.1021/cs4002699 | ACS Catal. 2013, 3, 1622−1632

The first patent for the direct synthesis of H_2O_2 was issued in 1914 for liquid-phase synthesis using a Pd catalyst.[10] Since then, many related investigations have aimed to develop more efficient processes for the direct synthesis of H_2O_2, often through the design of improved catalysts.[11−20] The addition of halide anions, specifically chloride and bromide, improves H_2O_2 yield on Pd catalysts.[16,17] Hutchings et al. demonstrated that alloying Pd with Au improves H_2O_2 selectivity and yield in the direct synthesis, even in the absence of halide ions.[18,19] Recently, Pd-based membrane catalysts have been examined for the direct synthesis of H_2O_2.[21−24] These H_2 impermeable membrane catalysts can operate at the desirable stoichiometric H_2/O_2 ratio thereby avoiding the hazards associated with explosive H_2/O_2 mixtures. A major drawback is that thin film Pd membranes form a brittle and catalytically inactive β-PdH phase.[25] Utilization of Pd alloys, including metals such as Cu, Ni, Fe, Pt, and Ag, is one means of preventing this problem, but identification of an alloy with desirable catalytic properties as well is an open research topic.[20,23,25,26]

The mechanism for oxygen reduction has been thoroughly studied on several monometallic and bimetallic catalysts using both experimental and theoretical methods.[27−30] In particular, recent theoretical studies have aimed to understand the remarkable reactivity and selectivity of PdAu catalysts.[31−34] The activation energy barriers and thermochemistry of elementary steps implicated throughout the literature in the H_2-O_2 reaction can be classified as hydrogenation steps and O−O bond scission steps:

Hydrogenation

$$O_2 + H \rightarrow OOH$$

$$OOH + H \rightarrow HOOH$$

$$O + H \rightarrow OH$$

$$OH + H \rightarrow H_2O$$

$$2OH \rightarrow H_2O + O$$

O−O Bond Scission

$$O_2 \rightarrow 2O$$

$$OOH \rightarrow OH + O$$

$$HOOH \rightarrow 2OH$$

For the direct synthesis of H_2O_2, a catalyst which prefers hydrogenation over O−O bond scission is required. Thus, bimetallic alloy catalysts composed of reactive transition metals, such as Pd or Pt, and less reactive noble metals that tend to suppress O−O bond scission, such as Au or Ag, could be potentially useful catalysts, as demonstrated by previous studies on PdAu.[18−20,29] In this work, we have performed a systematic density functional theory (DFT) investigation of O_2 reduction by H_2 on a Pd-noble metal alloy, PdAg, a catalyst widely studied for its application in hydrogenation reactions.[35−37] The minimum energy path in the reaction between H_2 and O_2 on monometallic Pd has been previously shown to lead to H_2O formation via OOH dissociation.[29] Therefore, suppressing this dissociation step by alloying with Ag, which exhibits a higher barrier for OOH dissociation similar to that of Au, might result in improved H_2O_2 selectivity.[29] The detailed thermochemistry of adsorption of hydrogen oxidation reactants and intermediates, namely, molecular oxygen (O_2), molecular hydrogen (H_2), atomic oxygen (O), atomic hydrogen (H), hydroxyl (OH), peroxyl (OOH), hydrogen peroxide (HOOH), and water (H_2O), on the close-packed (110) facet of PdAg is described in detail. Accordingly, the calculated energetics of the elementary steps discussed above, including activation energy barriers, are presented. These results are compared and contrasted with the analogous results recently reported by Ford et al. for the monometallic close-packed (111) surfaces of Pd and Ag[29] to illustrate the effect of alloying on the reaction energetics. The electronic characteristics of the metal atoms in the PdAg(110) surface, controlling the chemistry, are also discussed.

2. METHODS

DFT calculations are performed using DACAPO, a periodic, self-consistent total energy code.[38,39] The exchange-correlation functional is described by the generalized gradient approximation (GGA-PW91).[40] The electron-ion interactions are described by Vanderbilt ultrasoft pseudopotentials.[41] The electron wave function is expanded using plane waves with a kinetic energy cutoff of 25 Ry.[42] The self-consistent PW91 density is determined by iterative diagonalization of the Kohn−Sham Hamiltonian, Fermi population of the Kohn−Sham states (k_BT = 0.1 eV), and Pulay mixing of the resulting electronic density.[43] All total energies are extrapolated to k_BT = 0 eV. Because gas phase molecular oxygen carries a magnetic moment, calculations involving adsorbed molecular oxygen are performed spin-polarized, whereas all other calculations are not spin-polarized. The surface Brillouin zone is sampled with a 6 × 6 × 1 Monkhorst-Pack k point grid.

The PdAg surface is modeled by the (110) facet of the stable $L1_1$ phase of the PdAg bulk alloy (Figure 1b).[44,45] Our calculations show that this bimetallic surface is more stable than the (111) surface of PdAg, which contains monometallic layers. The surface is represented by a (2 × 2) four-layer slab, corresponding to 0.25 monolayer (ML) coverage for a single adsorbate in the unit cell, periodically repeated in a super cell geometry with successive slabs separated by six equivalent layers of vacuum. Adsorption is allowed on only one of the two exposed metal surfaces per slab, and the electrostatic potential is adjusted accordingly.[46,47] The optimized lattice parameter of the bulk alloy in the rhombohedral unit cell is calculated to be 4.95 Å and the angle is 33.51° (Figure 1a). The bottom two layers of the metal slab are fixed in their bulk truncated positions, whereas the top two layers are allowed to relax.

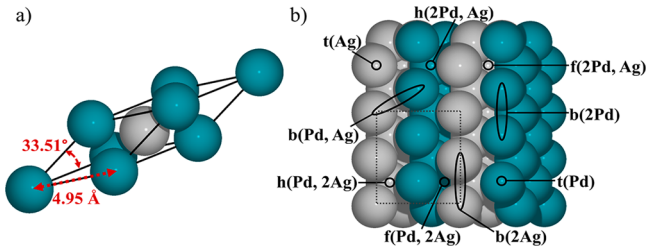

Figure 1. (a) Optimized rhombohedral unit cell for bulk $L1_1$ PdAg. (b) Top-view of the (110) facet of the $L1_1$ phase of PdAg. First letter of the adsorption site name indicates the geometry of the site: *f* = fcc, *h* = hcp, *t* = top, *b* = bridge; the surface atoms to which an adsorbate at the respective site is coordinated are listed inside the parentheses, Pd (green spheres) and Ag (gray spheres); dotted black line indicates the 2 × 2 surface unit cell.

The reported binding energies (BE) of adsorbates are calculated as

dx.doi.org/10.1021/cs4002699 | ACS Catal. 2013, 3, 1622−1632

$$BE = E_{total} - E_{substrate} - E_{gas}$$

where E_{total}, $E_{substrate}$, and E_{gas} are the total energies of the slab with the adsorbate, the metal slab without the adsorbate, and the adsorbate in the gas phase, respectively. Convergence of the total energy with respect to the k point set, energy cutoff, and the number of metal layers included is confirmed.

Minimum energy paths and activation energy barriers for all elementary steps are calculated using the climbing-image nudged elastic band (CI-NEB) method.[48] At least seven intermediate images are interpolated between reactant and product states. The transition state of the minimum energy path for each elementary step is confirmed by vibrational frequency calculations yielding a single imaginary frequency along the reaction coordinate. All reported binding energies, activation energy barriers, and reaction energies include zero-point energy corrections (ZPEC), which are calculated as ZPE = $\sum_i 1/2\ h\nu_i$, where i's correspond to the different vibrational modes and ν_i are the vibrational frequencies which are calculated by diagonalizing the mass-weighted Hessian matrix.[49]

3. RESULTS AND DISCUSSION

Adsorption of Reactants and Intermediates. The high symmetry adsorption sites on the PdAg(110) surface are shown schematically in Figure 1b and are analogous to those found on the close-packed (111) surface of a face-centered cubic (fcc) alloy. The nomenclature for adsorption sites used throughout the text indicates the site by the first single letter: fcc (f), hcp (h), bridge (b), and top (t). The metal atoms at the surface, including the number of each type, to which the adsorbate is coordinated are listed inside parentheses. A summary of the binding energies and preferred adsorption sites on PdAg(110), and those reported by Ford et al. on Pd(111) and Ag(111) for H_2*, H*, O*, OH*, and H_2O* can be found in Table 1. This data, with the addition of O−O bond distances and vibrational frequencies of the O−O vibrational modes, are listed for O_2*, OOH*, and HOOH* in Table 2. The adsorption geometry and thermochemistry of all intermediates on PdAg(110) are described in the following sections (3.1 and 3.2) and illustrated in Figure 2. The calculated activation energy barriers and reaction energies of elementary steps are discussed in a subsequent section (3.3). Detailed information describing the adsorption of intermediates on Pd(111) and Ag(111) have been previously described by Ford et al.[29] The computational tools and unit cell size used by Ford et al. are identical to those used in this study; however, the calculations in this study were completed with the top two layers of the slab relaxed, whereas calculations performed by Ford et al. are for static slabs. Yet, relaxation effects on the calculated adsorbate thermochemistry and activation energy barriers were shown to be minimal on Pt(111).[29]

Table 1. Preferred Adsorption Configurations and Corresponding ZPE-Corrected PW91 Adsorption Energies (BE) of H_2, O, H, OH, and H_2O on PdAg(110), Pd(111), and Ag(111) at 1/4 ML Coverage[a]

	PdAg(110)		Pd(111)[29]		Ag(111)[29]	
	site	BE (eV)	site	BE (eV)	site	BE (eV)
H_2	t(Pd)	−0.34				
O	f(2Pd, Ag)	−3.55	fcc	−3.64	fcc	−3.13
H	f(2Pd, Ag)	−2.65	fcc	−2.70	fcc	−1.92
OH	f(2Pd, Ag)	−2.33	br-tilted	−2.04	fcc	−2.28
H_2O	t(Pd)	−0.20	top	−0.21	top	−0.13

[a]Molecular hydrogen does not adsorb associatively on Pd(111) or Ag(111).

3.1. Adsorption of H_2*, H*, O*, OH*, and H_2O*. The preferred adsorption site for molecular hydrogen on PdAg(110) is at the t(Pd) site, binding through both H atoms (Figure 2), with a binding energy of −0.34 eV. The calculated H−H bond distance for adsorbed molecular hydrogen, H_2*, is 0.86 Å, which is elongated relative to the calculated bond distance in the gas phase (0.76 Å). This adsorption site is similar to H_2 adsorption on Pd(210) reported in the literature.[50] The relatively strong adsorption of H_2 to a metal is reminiscent of the adsorption of dihydrogen in inorganic Kubas complexes.[51] The binding energy of atomic hydrogen, H*, is −2.65 eV at a coverage of 0.25 ML. Atomic hydrogen is stable at each of the four high-symmetry 3-fold sites of PdAg(110) with similar binding strengths, but exhibits a slight preference for the f(2Pd, Ag) site. At a coverage of 0.5 ML on PdAg(110), the differential binding energy of the second H* is −2.54 eV, indicating a slight repulsion between H* at neighboring f(2Pd, Ag) sites. The preferential adsorption site for O* on PdAg(110) at 0.25 ML coverage is at the f(2Pd, Ag) site (Figure 2) with a binding energy of −3.55 eV. Atomic oxygen occupies the same surface site at 0.5 ML coverage; the differential binding energy for the second O* is −2.98 eV, indicating a more substantial repulsion between the two coadsorbed O*, compared to coadsorbed H* (see above).

In its most stable adsorbed state, hydroxyl, OH*, binds with an adsorption energy of −2.33 eV at the f(2Pd, Ag) site and with its O−H bond tilted away from the surface normal (Figure 2). At 0.5 ML coverage, the differential binding energy of the second OH* is −2.08 eV. The preferred binding site of both OH* at 0.5 ML coverage is the b(Pd, Ag) site. At this higher coverage the H of one OH* is tilted and oriented toward the O of the neighboring OH*, allowing for H-bonding between adjacent OH*s. The O−H bond length in OH* on PdAg(110), at coverages of 0.25 and 0.5 ML, is ∼0.98 Å. At 0.5 ML coverage, the stronger attraction of OH*, at the b(Pd, Ag) site, to Pd can be clearly noted by the Ag−OH bond length, 2.34 Å, versus the Pd−OH bond length of 2.12 Å.

H_2O* binds weakly to the surface with a binding energy of −0.20 eV. H_2O* binds through its oxygen atom and occupies a t(Pd) adsorption site (Figure 2). The optimized geometry for H_2O* yields the following results: O−H bond distances of ∼0.98 Å and an H−O−H angle of 104.3°. The bond angle and bond lengths of adsorbed water are virtually identical to the calculated gas phase values (O−H bond distances of 0.98 Å and an H−O−H angle of 104.3°).

3.2. Adsorption of O_2*, OOH*, and HOOH*. Molecular oxygen adsorbs on PdAg(110) with a binding energy of −0.60 eV at the top sites on two adjacent palladium atoms (Figure 2). The calculated O−O bond distance in the adsorbed molecule on PdAg(110) is 1.32 Å. Compared with the calculated gas phase O−O bond length of 1.23 Å, the elongation of the molecular bond in O_2* is similar to that found for H_2*. Molecular oxygen adsorbed on PdAg(110) carries 1.08 μ_B of magnetic moment, compared to 2.0 μ_B in the gas phase.

The binding energy of the peroxyl intermediate, OOH*, is −1.18 eV. The most stable configuration is at a b(2Pd)-t(Ag) site. This configuration has the OOH* bound through the non-hydrogenated O end at a b(2Pd) site with the OH end tilted away from the surface, creating an overall tilted state (Figure 2).

dx.doi.org/10.1021/cs4002699 | ACS Catal. 2013, 3, 1622−1632

Table 2. Preferred Adsorption Configurations and Corresponding ZPE-Corrected PW91 Binding Energies (BE), O−O Bond Lengths (d_{O-O}), and Frequency of the O−O Vibrational Modes (ν_{O-O}) of O_2, OOH, and HOOH on PdAg(110), Pd(111), and Ag(111)

	site	BE (eV)	d_{O-O} (Å)	ν_{O-O} (cm^{-1})
PdAg(110)				
O_2	t(Pd)-t(Pd)	−0.60	1.32	1065
OOH	b(2Pd)-t(Ag)	−1.18	1.51	710
HOOH	t(Pd)-f(2Pd, Ag), t(Pd)-h(2Pd, Ag)	−0.33	1.48	821
Pd(111)[29]				
O_2	top-br	−0.50	1.35	928
OOH	bent top	−0.96	1.46	704
HOOH		−0.30	1.48	843
Ag(111)[29]				
O_2	top-top	−0.12	1.30	1149
OOH	bent br	−1.01	1.50	784
HOOH		−0.18	1.47	878

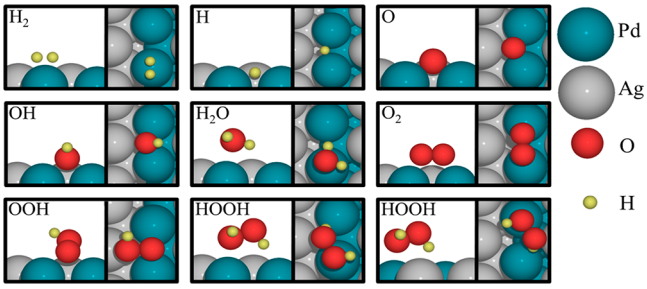

Figure 2. Minimum energy adsorption modes (cross section, left panel; and top view, right panel) for the individual adsorbates on PdAg(110). Small yellow, medium red, and large gray and green spheres represent H, O, Ag, and Pd atoms, respectively.

The OH end lies above a t(Ag) site. The calculated O−OH bond length in OOH* at the b(2Pd)-t(Ag) site is 1.50 Å.

The interaction of hydrogen peroxide, HOOH*, with the surface is weak; the binding energy is −0.33 eV. Two isoenergetic adsorption sites were identified as the preferred sites: t(Pd)-f(2Pd, Ag) and t(Pd)-h(2Pd, Ag) (Figure 2). HOOH* exhibits a similar geometry in both configurations, with the adsorbed molecule interacting more closely with the Pd atoms. Similar to the most stable configuration on many monometallic surfaces, HOOH* adsorbs on PdAg in a *trans* configuration, with one OH group bound at a top site and the H on the other OH group tilted toward the surface, residing above a hollow site. The calculated HO−OH bond length is 1.48 Å, which is identical to the bond distance calculated for HOOH in the gas phase.

On PdAg(110), Pd(111), and Ag(111) the vibrational frequencies of the O−O stretching mode of adsorbed O_2, OOH, and HOOH all increase in the order OOH < HOOH < O_2. All of these O−O stretching modes are dipole-active and therefore, in principle, could be detected using vibrational spectroscopy. A detailed discussion of studies identifying these dioxygen intermediates on various monometallic metal surfaces can be found in ref 29.

Table 3. ZPE-Corrected PW91 Activation Energy Barriers (E_A) and Reaction Energies (ΔE) for All Elementary Steps[a]

	PdAg(110)		Pd(111)[29]		Ag(111)[29]	
elementary step	E_A (eV)	ΔE (eV)	E_A (eV)	ΔE (eV)	E_A (eV)	ΔE (eV)
$H_2 \rightarrow H + H$	0.09	−0.66	0.00	−0.96	1.04[b]	0.34
		(−0.45)		(−0.83)		(0.29)
$O_2 \rightarrow O + O$	1.06	0.75	0.84	−0.67	1.22	0.43
		(−0.82)		(−1.23)		(−0.60)
$O_2 + H \rightarrow OOH$	0.75	−0.19	0.63	0.04	0.20	−1.06
	(0.92)	(−0.12)	(0.80)	(0.21)	(0.26)	(−1.00)
$OOH \rightarrow OH + O$	0.26	−0.98	0.06	−1.18	0.41	−0.61
	(0.44)	(−1.42)		(−1.53)		(−1.19)
$OOH + H \rightarrow HOOH$	0.68	−0.29	0.40	−0.25	0.60	−0.78
	(0.91)	(−0.06)	(0.60)	(−0.04)	(0.71)	(−0.66)
$HOOH \rightarrow OH + OH$	0.20	−1.83	0.19	−1.39	0.18	−2.06
		(−2.07)		(−1.59)		(−2.11)
$O + H \rightarrow OH$	0.74	−0.73	0.72	−0.31	0.36	−1.89
	(0.80)	(−0.72)	(0.95)	(−0.08)	(0.66)	(−1.59)
$OH + H \rightarrow H_2O$	0.62	−0.33	0.39	−0.58	0.48	−0.92
	(0.66)	(−0.28)	(0.58)	(−0.38)	(0.63)	(−0.83)
$OH+OH \rightarrow H_2O + O$	0.27	−0.08	0.00	−0.35	0.25	0.23
	(0.52)	(0.43)	(0.00)	(−0.30)	(0.31)	(0.76)

[a]The values without (with) parentheses are based on the reactant or product states used in the NEB calculation of the minimum energy path (infinitely far apart). [b]The reported activation energy barrier for H_2 dissociation on Ag(111) is from ref 54.

dx.doi.org/10.1021/cs4002699 | ACS Catal. 2013, 3, 1622−1632

3.3. Elementary Steps. The calculated activation energy barriers (E_A) and reaction energies (ΔE) of the elementary steps are reported in Table 3, and the initial state, transition state, and final state of each step are illustrated in Figure 3. For

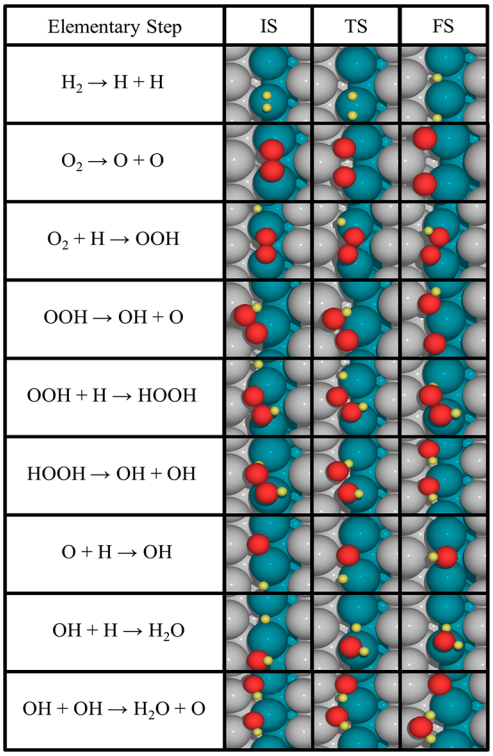

Figure 3. Configurations of the calculated initial state (IS), transition state (TS), and final state (FS) of the elementary steps on PdAg(110). IS and FS depict the state used in the NEB calculation. Yellow, red, gray, and green spheres represent H, O, Ag, and Pd, respectively.

comparison, the activation energy barriers and reaction energies reported for the Pd(111) and Ag(111) surfaces by Ford et al.[29] are also included in Table 3. All activation energy barriers and reaction energies reported in the following text are calculated relative to the coadsorbed reactant or product states used in the NEB calculation for the minimum energy path. The respective energetics based on infinitely separated reactants and products are reported in Table 3 along with the coadsorbed values.

H_2 → H* + H**. H_2* dissociation proceeds directly from the most stable, though weakly bound, t(Pd) adsorption site on PdAg(110). At the transition state (Figure 3), the H−H bond length is 0.95 Å, which is 0.09 Å longer than the bond length in the molecularly adsorbed state. The dissociation of H_2* is a facile step on PdAg(110), with an activation energy of only 0.09 eV and a reaction energy of −0.66 eV, in general agreement with the use of PdAg in hydrogen storage and hydrogenation applications.[52,53] Hydrogen dissociation is spontaneous (E_A = 0 eV) on Pd(111) with a reaction energy of −0.96 eV. In contrast, this is a highly activated (E_A = 1.04 eV)[54] and endothermic (ΔE = 0.34 eV) elementary step on Ag(111).

O_2 → O* + O**. The minimum energy path for direct O_2* dissociation begins with O_2* in its minimum energy state (t(Pd)-t(Pd), BE = −0.60 eV). The dissociation proceeds with stretching of the O−O bond above an f(2Pd, Ag) site, such that each O atom is near a Pd−Ag bridge site at the transition state (Figure 3). This geometry of the transition state is in agreement with experiments conducted on $Pd_{67}Ag_{33}$(111), which suggest that O_2 dissociation requires at least two neighboring Pd atoms.[55] The O−O bond length at the transition state is 1.98 Å. The two O* then settle at neighboring h(Pd, 2Ag) sites, an intermediate stable state along the reaction pathway, before diffusing to the most stable final state with both O* at neighboring f(2Pd, Ag) sites. The activation energy barrier for this O−O bond-breaking step is 1.06 eV, and the reaction energy is 0.75 eV (endothermic). This step has a lower barrier on Pd(111) (E_A = 0.84 eV) and a higher barrier on Ag(111) (E_A = 1.22 eV). However, the step is more endothermic on PdAg(110) than on either Pd(111) (ΔE = −0.67 eV) or Ag(111) (ΔE = 0.43 eV). The minimum energy path for direct O_2* dissociation on PdAg(110) differs from that on Pd(111) and Ag(111), where O−O bond scission occurs above an hcp site. As a result, whereas the geometry of the most stable, coadsorbed final state on all three surfaces is identical (2 fcc sites), the pathway on PdAg(110) goes through the intermediate hcp-hcp (h(Pd, 2Ag)-h(Pd, 2Ag)) state. This h(Pd, 2Ag) site for coadsorbed O* (0.5 ML) on PdAg(110) is 1.14 eV less stable than the most stable f(2Pd, Ag) site.

O_2 + H* → OOH**. In the initial state for peroxyl formation, O_2* and H* are coadsorbed in their most stable binding sites at infinite separation, t(Pd)-t(Pd) and f(2Pd, Ag), respectively. As the step proceeds, the OO—H bond forms at a t(Pd) site (Figure 3). In the final state of the minimum energy path the OOH* intermediate is at a b(Pd, Ag)-t(Pd) site, which is 0.10 eV less stable than the most stable b(2Pd)-t(Ag) site. The activation energy barrier for this step is 0.75 eV, and the reaction energy is −0.19 eV. This step is more energetically favorable on Ag(111) (E_A = 0.20 eV, ΔE = −1.06 eV). On Pd(111), the activation barrier for the peroxyl formation elementary step is lower (E_A = 0.63 eV) than that on PdAg(110), but the reaction energy is less favorable (ΔE = 0.04 eV). On Ag(111) this step begins with O_2 in the gas phase, as O_2 does not bind on the Ag(111) surface in the presence of 0.25 ML H*.

OOH → OH* + O**. The minimum energy pathway for breaking the O−O bond in OOH* begins with OOH* in the b(Pd, Ag)-t(Ag) site, which is 0.17 eV higher in energy than the most stable adsorption site, b(2Pd)-t(Ag). The bond-breaking occurs around the Pd atom separating the OH* and O* in the final state (Figure 3). The elementary step ends with OH* and O* in the b(Pd, Ag) and f(2Pd, Ag), respectively. This final state is 0.13 eV higher in energy than the most stable coadsorbed final state, in which both adsorbates occupy f(2Pd, Ag) sites. The activation energy barrier and reaction energy for this step, 0.26 eV and −0.98 eV, respectively, fall between the respective values on Pd(111) and Ag(111). This step is more energetically favorable on Pd(111) (E_A = 0.06 eV, ΔE = −1.18 eV) and less favorable on Ag(111) (E_A = 0.41 eV, ΔE = −0.61 eV).

OOH + H* → HOOH**. The minimum energy pathway for OOH* hydrogenation to H_2O_2 requires the OOH* to first diffuse, via a rotation, from the most stable b(2Pd)-t(Ag) site to the b(Pd, Ag)-t(Pd) site. H* begins in its most stable f(2Pd, Ag) site. The H* approaches the OOH* from the same side as the H atom in OOH*, resulting in a *cis* configuration of the complex at the transition state (Figure 3). Interestingly, this contrasts with the *trans* configuration of the transition state complex in the same step on Pd(111) and Ag(111), where the H approaches OOH* from the opposite side of the H in OOH*. The barrier for this step, 0.68 eV, is higher than the barrier on Pd(111), 0.40 eV, and on Ag(111), 0.60 eV. The

dx.doi.org/10.1021/cs4002699 | ACS Catal. 2013, 3, 1622−1632

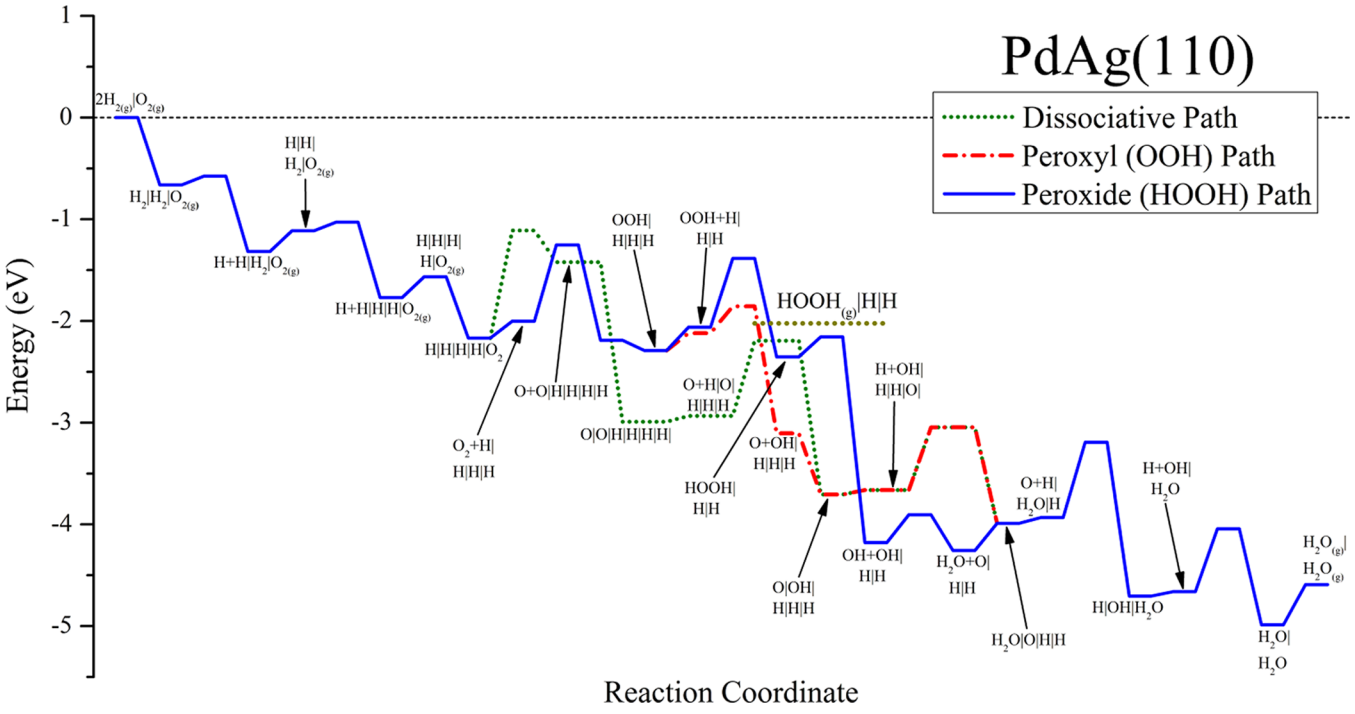

Figure 4. 2D Potential energy surface diagram of the hydrogen−oxygen reaction via the dissociative, peroxyl and peroxide mechanisms on PdAg(110). Zero-energy corresponds to the energy of two H_2 and one O_2 in the gas phase. All non-gas-phase states are adsorbed, but the * is omitted for brevity. Adsorbates connected by "+" are coadsorbed; those connected by "|" are at infinite separation.

final state for HOOH* in this step is one of the two isoenergetic most stable states, t(Pd)-f(2Pd, Ag), and is similar to the most stable configuration of HOOH* on Pd(111) and Ag(111). This step, with a reaction energy of −0.29 eV on PdAg(110), is slightly less exothermic on Pd(111) (ΔE = −0.25 eV) and significantly more exothermic on Ag(111) (ΔE = −0.78 eV).

*HOOH** → *OH** + *OH**. HOOH* begins in its most stable t(Pd)-f(2Pd, Ag) site, and the O—O bond breaks across a b(Pd, Ag) site (Figure 3). At the transition state, the H in both OH* groups are directed toward neighboring Pd atoms. The activation energy barrier for this step, 0.20 eV, is comparable to that on Pd(111) and Ag(111), 0.19 and 0.18 eV, respectively. The step proceeds, following the transition state, with both OH* groups rotating into their most stable coadsorbed configuration at neighboring b(Pd, Ag) sites. The final NEB coadsorbed state is analogous to that on Ag(111), but differs from the 0.5 ML OH* state on Pd, where both OH* occupy top sites. With a reaction energy of −1.83 eV, this step is the most exothermic elementary step considered in this study. This step is similarly a highly exothermic step on Pd(111) (ΔE = −1.39 eV) and Ag(111) (ΔE = −2.06 eV).

*O** + *H** → *OH**. Hydroxyl formation from O* and H* begins with O* and H* in neighboring f(2Pd, Ag) sites. This initial state is analogous to that on Pd(111), but differs from Ag(111) where H* occupies an hcp site in the most stable coadsorbed configuration. The transition states on all three surfaces are quite similar, with the H* at an hcp site and the O* in an fcc site (Figure 3). Following formation of the O−H bond, OH* is in an intermediate stable b(2Pd) state with the H oriented above an f(2Pd, Ag) site. The OH* must then rotate to reach its final, most stable state, f(2Pd, Ag), with the H oriented above a b(2Pd) site. In both the intermediate minimum energy state and the final, most stable state for OH*, the O−H bond is tilted with respect to the surface plane. The activation barrier on PdAg(110) (E_A = 0.74 eV) is similar to the barrier on Pd(111) (E_A = 0.72 eV), despite the increased exothermicity on PdAg(110) (ΔE = −0.73 eV) compared with Pd(111) (ΔE = −0.31 eV). On Ag(111), this step is significantly more exothermic (ΔE = −1.89 eV) and has a much lower barrier (E_A = 0.36 eV).

*OH** + *H** → *H*$_2$*O**. In the initial state for water formation from OH* and H* the adsorbates are in their most stable coadsorbed configuration: OH* occupies an f(2Pd, Ag) site and H* occupies the neighboring b(2Pd) site. In contrast, on both Pd(111) and Ag(111), the coadsorbed initial state consists of OH* at a top site and H* at an fcc site. On PdAg(110), at the transition state, the OH* is at a t(Pd) site next to the H* (Figure 3). In the final state H_2O* is at its most stable, t(Pd) site. The activation energy barrier is 0.62 eV, and the reaction energy is −0.33 eV. This step is less energetically favorable on PdAg(110) than on either Pd(111) or Ag(111); it has a higher barrier and is less exothermic on PdAg(110). The activation energy barrier and reaction energy on Pd(111) are 0.39 eV and −0.58 eV and on Ag(111) are 0.48 eV and −0.92 eV, respectively.

*OH** + *OH** → *H*$_2$*O** + *O**. On PdAg(110), the preferential sites for coadsorbed OH* at 0.5 ML coverage are neighboring b(Pd, Ag) sites. This state is the initial state in the minimum energy path for hydroxyl disproportionation to form H_2O* and O*. At the transition state, one of the OH* has shifted to an f(2Pd, Ag) site closer to the OH* at the neighboring b(Pd, Ag) site (Figure 3). This transition state is similar to that found on Ag(111). In the final state, H_2O* and O* are coadsorbed on PdAg(110) with the H_2O at a t(Ag) site and the O* at an f(2Pd, Ag) site. The activation energy barrier on PdAg(110) is 0.27 eV, similar to the barrier on Ag(111), 0.25 eV. This step is more exothermic on PdAg(110), with a reaction energy of

dx.doi.org/10.1021/cs4002699 | ACS Catal. 2013, 3, 1622−1632

−0.08 eV, compared to the endothermic reaction energy of 0.23 eV on Ag(111). In contrast, this step is spontaneous (E_A = 0 eV) and exothermic (ΔE = −0.35 eV) on Pd(111).

3.4. Potential Energy Surfaces. The elementary steps described can be combined to form one dissociative and two associative ORR mechanisms. The *dissociative* path involves the direct dissociation of O_2 after its adsorption, followed by two hydrogenation steps to yield H_2O. The first associative pathway, the *peroxyl* path, involves the hydrogenation of O_2* to OOH*, followed by its dissociation to O* and OH*, and subsequent hydrogenation of these species to produce H_2O. In the second associative path, the *peroxide* path, O_2* is hydrogenated to OOH* which then undergoes a second hydrogenation to form HOOH*. The HOOH* can then either desorb (making this the selective pathway for the direct synthesis of hydrogen peroxide) or dissociate to yield two OH*. These two OH* species can then undergo a disproportionation step to form H_2O* and O*. To complete the catalytic cycle, the O* can undergo two hydrogenation steps to form H_2O. The reaction between HOOH* and H* to form H_2O and OH* is an alternative peroxide decomposition step. Li et al. included this elementary step in their study of hydrogen peroxide decomposition on Pd(111) and found that the high activation barrier for this step made it very unfavorable compared with direct decomposition of HOOH*.[32] In this study, all attempts to model this step converged to 2OH* + H*, suggesting that peroxide hydrogenation and dissociation to form H_2O and OH* is not an elementary step on PdAg(110). Ford et al. considered the hydrogenation of HOOH* to HOOHH*, but did not find this to be a stable intermediate on any of the five monometallic sufaces studied, including Pd(111) and Ag(111).[29] The energetics associated with the aforementioned competing mechanisms are shown in the complete potential energy surface (PES) for oxygen reduction on PdAg(110) in Figure 4.

The transition state energy for the direct dissociation of O_2* is higher in energy than the hydrogenation of O_2* to form OOH*, suggesting that based on the PES an associative path should be preferred on PdAg(110). All steps following the O−O bond breaking step in the dissociative path are energetically easier than the O_2* dissociation step, indicating that this step is key in determining the selectivity between the associative paths and the dissociative path. In particular, this step has the highest barrier of any step in all three mechanisms. The associative paths will also compete with O_2* desorption, which is energetically more favorable by 0.15 eV compared with O_2* hydrogenation. Along the associative paths, peroxyl formed via O_2* hydrogenation can either dissociate to form OH* and O* or undergo hydrogenation to form HOOH*. On PdAg(110), the O−OH* dissociation reaction has a significantly lower barrier (E_A = 0.26 eV) and is much more exothermic (ΔE = −0.98 eV) than the competing hydrogenation step (E_A = 0.68 eV, ΔE = −0.29 eV). Dissociation of OOH* eventually leads to H_2O. Following the PES along the peroxide pathway, despite the fact that this path appears to be energetically less favorable, results in the formation of HOOH* that is highly susceptible to decomposition to produce two OH*. The barrier for HO−OH* dissociation is only 0.20 eV, and this is the most exothermic step in all three mechanisms. The desorption energy of HOOH* is 0.33 eV, which is 0.13 eV higher than the energy required to dissociate HOOH*, further demonstrating that even if HOOH* is produced on PdAg(110) it is unlikely to desorb as a gas phase product; it will rather decompose. Thus, based on the PES the minimum energy path for the hydrogen−oxygen reaction on PdAg(110) leads to water formation rather than H_2O_2, and H_2O production likely proceeds through the associative, peroxyl, mechanism.

A comparison of the overall PES on PdAg(110) and those on Pd(111) and Ag(111)[29] reveals that on all three surfaces hydrogenation of O_2* is more favorable than direct dissociation. Along the associative paths, the energetics of peroxyl hydrogenation and peroxyl dissociation can therefore be compared to predict the relative selectivity toward peroxide versus water on all three surfaces. As shown in Figure 5, on PdAg(110), Pd(111), and Ag(111) the barrier for HOOH* formation via OOH* hydrogenation is 0.47 eV, 0.55 eV, and 0.31 eV higher than the barrier for OOH* dissociation,

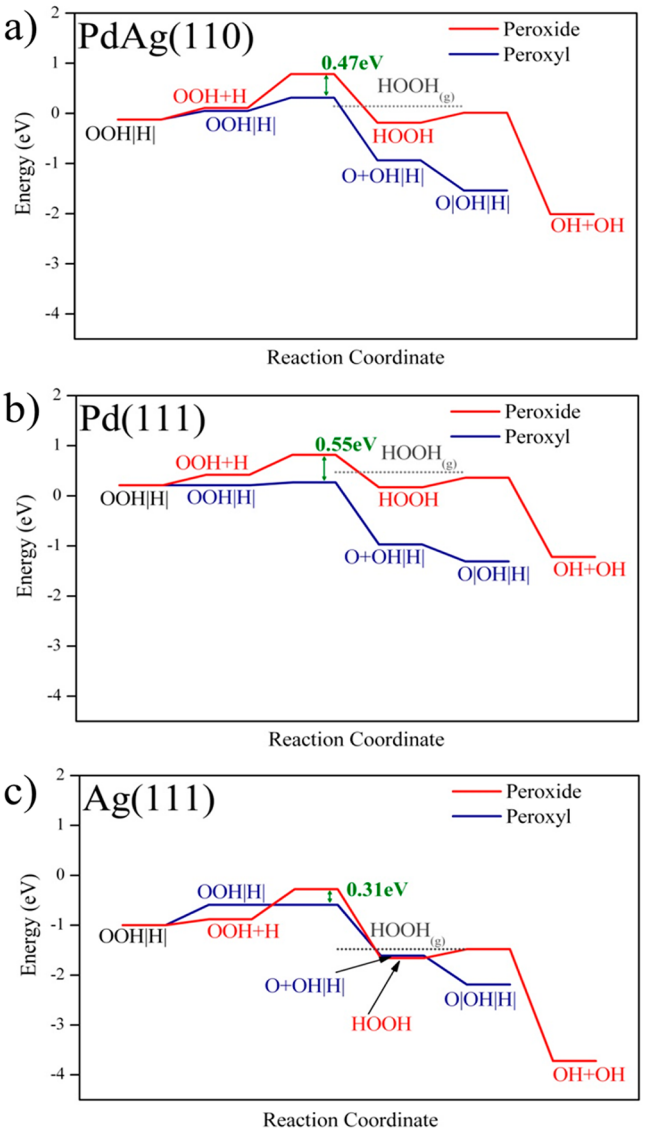

Figure 5. 2D PES for the selectivity determining steps along the two associative pathways: peroxide path (red) and peroxyl path leading to water (blue). The value reported in green indicates the difference between the transition state energy for peroxyl hydrogenation to hydrogen peroxide and peroxyl dissociation to O+OH. All non-gas-phase states are adsorbed, but the * is omitted for brevity. Adsorbates connected by "+" are coadsorbed; those connected by "|" are at infinite separation.

dx.doi.org/10.1021/cs4002699 | ACS Catal. 2013, 3, 1622−1632

respectively. Thus, although alloying with Ag decreased the barrier for OOH* dissociation, the relatively small decrease combined with a slight increase in the barrier for OOH* hydrogenation resulted in an overall decrease in the predicted H_2O_2 selectivity. Based on this key selectivity parameter, Ag(111) is expected to display the highest selectivity toward H_2O_2, though the selectivity may still be quite low because of facile decomposition of any H_2O_2 formed.[56,57] This is a particularly useful comparison as the magnitude of the barriers for H_2O_2* decomposition and the desorption energies are similar on all three surfaces.

To compare the reactivity of PdAg(110), Pd(111), and Ag(111), the PES for each of the dissociative, peroxyl and peroxide pathways, generated using the data on Pd(111) and Ag(111) from Ford et al.,[29] are shown in Figure 6a, 6b, and 6c, respectively. Inspection of the PESs shows that while the PdAg(110) PES generally falls between that of monometallic

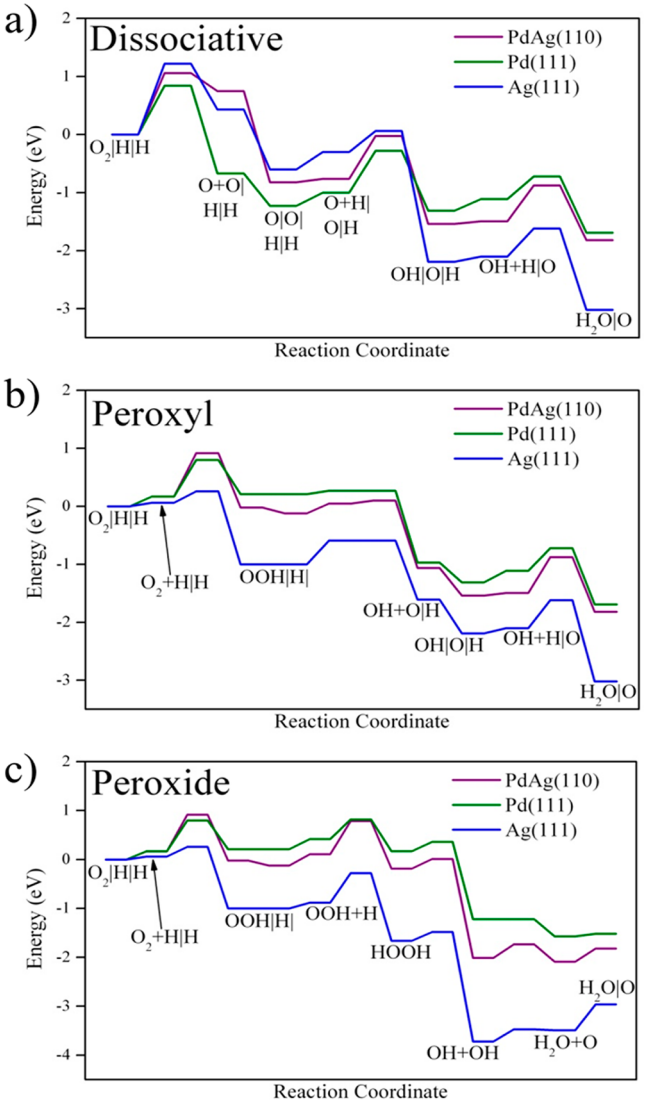

Figure 6. 2D Potential energy surface for the ORR on PdAg(110), Pd(111), and Ag(111) via the (a) dissociative, (b) peroxyl, and (c) peroxide path. The PESs include only the section along the reaction coordinate in Figure 4 that determines selectivity. All species indicated are adsorbed on the metal surface. Adsorbates connected by "+" are coadsorbed; those connected by "|" are at infinite separation.

Pd(111) and monometallic Ag(111), the energetics along each of the three pathways on PdAg(110) follow Pd(111) more closely. This is in agreement with the observation, throughout the reported results, that all adsorbates and transition states on PdAg(110) generally lie closer to the Pd atoms of that surface. Specifically, both of the associative paths on PdAg(110) and Pd(111) are quite similar.

To further explore similarities and differences in reactivity between PdAg(110), Pd(111), and Ag(111), we calculated the d-band center (ε_d), with respect to the Fermi level, of the Pd and Ag surface atoms in PdAg(110) and several facets of monometallic Pd and Ag (Table 4). The d-band center of Pd in

Table 4. d-Band Center (ε_d) of Surface Atoms at Various Sites in PdAg(110), Pd(111), Pd(100), Pd(211), Ag(111), and Ag(211)

surface	site	ε_d (eV)
Pd(111)	terrace	−1.82
Pd(100)	terrace	−1.73
Pd(211)	step edge	−1.71
Pd(211)	terrace	−1.88
Pd(211)	step foot	−1.98
Ag(111)	terrace	−4.12
Ag(211)	step edge	−4.09
Ag(211)	terrace	−4.16
Ag(211)	step foot	−4.22
PdAg(110)	Pd-terrace	−1.68
PdAg(110)	Ag-terrace	−3.63

PdAg(110) (ε_d = −1.68 eV) shifts up relative to that of monometallic Pd(111) (ε_d = −1.82 eV), as shown in other studies of PdAg alloys.[26] Likewise, the d-band center of Ag in PdAg(110) (ε_d = −3.63 eV) is higher than that in monometallic Ag(111) (ε_d = −4.12 eV). This upshift of the d-band center in Ag is somewhat surprising, as alloying a noble metal with a transition metal generally results in loss of charge by the noble metal, and thus, a downshift in the d-band center. It has been previously demonstrated that in PdAg alloys, both Pd and Ag gain d and lose non-d (s and p) charge.[26,58] The charge loss in Ag is only partially compensated by d-charge gain, resulting in the expected overall loss of charge despite the upshift of the d-band center. The higher lying d-band centers of Pd and Ag correspond to an increase in the reactivity of the Pd and Ag atoms in PdAg(110) compared to the respective atoms' reactivity in their monometallic close-packed surface. Comparison of the shift of the d-band center for Pd versus Ag indicates that alloying Pd and Ag has more significantly altered the reactivity of the Ag atoms. In fact, if one compares the d-band center of the Ag atoms in the PdAg(110) alloy with the d-band center of step edge atoms on the (211) facet of Ag, the increased reactivity exceeds even under-coordinated step sites of Ag. Further, the significantly higher-lying d-band center of the Pd atoms in PdAg(110) compared to the Ag atoms in PdAg(110) indicates that the Pd surface atoms should be much more reactive than the Ag atoms. Comparison of the d-band center of the Pd atoms in PdAg(110) with the d-band center of Pd atoms in the more open (100) and stepped (211) monometallic Pd surfaces shows that the d-band center of Pd in PdAg(110) is quite similar to that of the under-coordinated Pd atoms located at the step sites in Pd(211). Inspection of the preferred adsorption sites (Figure 2) and elementary step transition state geometries (Figure 3) demonstrates that the

dx.doi.org/10.1021/cs4002699 | ACS Catal. 2013, 3, 1622−1632

surface chemistry not only prefers to occur near Pd atoms but also has a preference for the side of the Pd atoms where the fcc sites are coordinated by two Pd atoms, as opposed to two Ag atoms. The preference of adsorbates and coadsorbates to occupy fcc sites coordinated by two Pd atoms rather than two Ag atoms is a result of the higher d-band center of the Pd atoms. The average d-band center for 3-fold sites coordinated by two Pd atoms and one Ag atom is −2.33 eV, whereas the average d-band center of 3-fold sites coordinated by two Ag atoms and one Pd atom is −2.98 eV. Since the preferred initial and final states for reactants, intermediates, and products lie in these sites, the surface reactions generally proceed in the same region of the surface. Thus, the Pd atoms in PdAg(110) behave like 1D arrays of more active surface sites, illustrated in Figure 7, dominating the surface chemistry, similar to under-coordinated step sites.[59] In essence, the chemistry occurring on the bimetallic PdAg(110) surface has a dimensionality between that on typical monometallic surfaces (2D chemistry) and the 0D, noncontiguous surface chemistry observed, for example, by Chen et al. for acetoxylation of ethylene to vinyl acetate on surfaces containing Pd monomers surrounded by Au.[60] Another example of 1D surface chemistry has been recently described by Zhong et al.[61] for the polymerization of linear alkanes in 1D channels on the reconstructed Au(110) surface. However, in the case presented here the anisotropy of the surface, facilitating the 1D surface chemistry, is due to the bimetallic composition rather than the atomic scale structure of the surface.

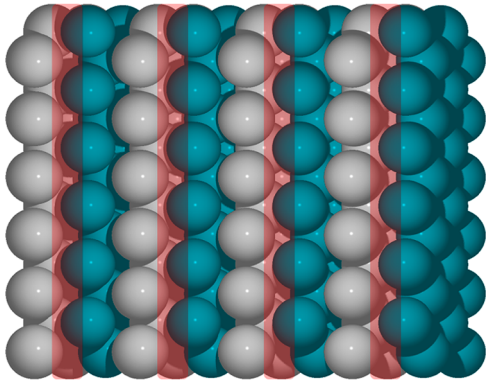

Figure 7. (110) Facet of PdAg: Pd (green spheres) and Ag (gray spheres). The regions shaded in red indicate the 1D arrays of active sites on the bimetallic surface.

It is likely that changes in the relative elemental surface composition (Pd:Ag) would create a more significant variation between the three PESs discussed above. In PdAg alloys under vacuum, it has been shown that Ag atoms prefer to segregate to the surface creating a surface that is almost exclusively dominated by Ag.[62−64] However, the presence of surface adsorbates, for example H* or O*, can induce surface segregation of Pd because of the stronger interaction between Pd and the adsorbates, as compared with Ag and those adsorbates.[63,65−67] These two competing factors make it difficult to determine the exact surface composition for PdAg under realistic reaction conditions. The presence of surface ensembles and variations in the composition of the subsurface layers can also alter the local reactivity of Pd surface atoms in PdAg alloys.[26] For this reason, theoretical studies of the direct synthesis of hydrogen peroxide on PdAu have been conducted on a variety of surface compositions.[31,33,34] Of these, a surface consisting of Pd monomers surrounded by Au on a Pd substrate best supports the experimental results showing improved H_2O_2 yield and selectivity on PdAu.[33] These ensembles of Pd monomers in Au are effective at suppressing O−O bond scission in all three reaction intermediates: O_2, OOH, and HOOH.[33,34] Thus, successfully coupling the high reactivity of Pd and the suppression of O−O bond scission predicted for Au in the bimetallic alloy to generate a highly selective active site is governed by the particular composition of the surface. A similar study of Pd monomers surrounded by Ag might therefore yield significantly different results than those presented here.

In closing, we note that more meaningful insights into the reactivity and selectivity of the H_2−O_2 reaction on Pd and Ag compared with PdAg could be obtained from a combined experimental and microkinetic modeling study of the reaction, similar to previous investigations conducted, for instance, for the water gas shift on Cu and Pt.[68,69] Additionally, conclusions drawn here for Pd, Ag, and PdAg as catalysts for the H_2−O_2 reaction are based on 1/4 ML coverage for all adsorbates. Higher coverages, which may reflect realistic reaction conditions more accurately, may drastically change the reaction energetics and selectivities.[70,71] In addition, liquid phase direct synthesis of H_2O_2 presents additional mechanistic challenges, including the interaction of intermediates and transition states discussed above with solvent molecules. Insights derived here might serve only as a basis for extending the fundamental understanding needed in more complicated reaction environments.

4. CONCLUSIONS

A systematic DFT investigation of the hydrogen−oxygen reaction on a model PdAg(110) surface has been performed, allowing for a comparison of the competing reaction mechanisms on the alloy surface with those on Pd(111) and Ag(111). The results show that alloying Pd and Ag shifts the d-band center of both metals in the surface upward, and this effect is more significant for the Ag atoms. The Ag atoms in PdAg(110) are found to be more reactive than even under-coordinated step edge atoms in Ag(211). Still, the d-band center of the Pd surface atoms remain much higher than the Ag surface atoms. Consequently, the stronger interaction between intermediates and Pd, compared to the relatively weak interaction with Ag, is translated into the preferred location of intermediates and transition states on the alloy surface. In particular, this is demonstrated by the preference of all intermediates to bind at sites which maximize the interaction with the Pd atoms in the alloy surface. The transition states of elementary steps also adopt geometries that maximize coordination with Pd atoms, and thereby the stabilization by Pd. Thus, the Pd atoms in PdAg(110) form 1D arrays of more active surface sites, dominating the surface chemistry, similar to under-coordinated step sites or missing row reconstructions in monometallic Pd surfaces. This results in a PES for the hydrogen−oxygen reaction on PdAg(110) which can be closely described by the respective PES on Pd(111). Thus, at a one to one, Pd to Ag, surface composition the effect of Ag on the reaction energetics is fairly small.

The PES on PdAg(110) shows that direct oxygen dissociation is more difficult than hydrogenation of adsorbed molecular oxygen. Therefore, based on the PES, the associative paths should be preferred. The associative path leading to

dx.doi.org/10.1021/cs4002699 | ACS Catal. 2013, 3, 1622−1632

hydrogen peroxide production is unlikely to be favorable because hydrogenation of the peroxyl intermediate is much more difficult than its dissociation. Furthermore, any hydrogen peroxide produced is likely to decompose rather than desorb. Based on a comparison of the reaction energetics, Ag(111) is predicted to be more selective toward H_2O_2 than either PdAg(110) or Pd(111), as Ag(111) is most effective at suppressing O−O bond scission. These results suggest that the bimetallic PdAg alloy is unlikely to be an effective catalyst for the direct synthesis of hydrogen peroxide. However, variations in the alloy composition of PdAg, particularly in the surface layer, may lead to improved H_2O_2 selectivity, as demonstrated in previous studies of PdAu. Thus, the reactivity of PdAg alloys for the direct synthesis of H_2O_2 may merit further experimental and theoretical studies.

AUTHOR INFORMATION

Corresponding Author

*E-mail: manos@engr.wisc.edu.

Notes

The authors declare no competing financial interest.

ACKNOWLEDGMENTS

We gratefully acknowledge the financial support of the U.S. Department of Energy, Basic Energy Sciences. C.A.F. thanks NSF for a Graduate Research Fellowship under Grant DGE-0946806. A.G.-G. acknowledges financial support from the National Science and Technology Council of Mexico, CONACYT (ref. 83247). The computational work was performed in part using supercomputing resources from the following institutions: EMSL, a National scientific user facility at Pacific Northwest National Laboratory (PNNL); the Center for Nanoscale Materials at Argonne National Laboratory (ANL); and the National Energy Research Scientific Computing Center (NERSC). EMSL is sponsored by the Department of Energy's Office of Biological and Environmental Research located at PNNL. CNM and NERSC are supported by the U.S. Department of Energy, Office of Science, under contracts DE-AC02-06CH11357 and DE-AC02-05CH11231, respectively.

REFERENCES

(1) Döbereiner, J. W. *Schweigg J.* **1923**, *39*, 1.
(2) Somorjai, G. A.; Li, Y. *Introduction to Surface Chemistry and Catalysis*, 2nd ed.; John Wiley & Sons, Inc.: Hoboken, NJ, 2010.
(3) Vielstich, W.; Lamm, A.; Gasteiger, H. A. *Handbook of Fuel Cells: Fundamentals, Technology, Applications*; Wiley: West Sussex, U.K., 2003.
(4) Adzic, R. R. Electrocatalysis. In *Frontiers in Electrochemistry*; Lipkowski, J., Ross, P. N., Eds.; Springer: Berlin, Germany, 1998; Vol. 5, p 197.
(5) Zhang, J.; Sasaki, K.; Sutter, E.; Adzic, R. R. *Science* **2007**, *315*, 220−222.
(6) Wang, Y. X.; Balbuena, P. B. *J. Phys. Chem. B* **2005**, *109*, 18902−18906.
(7) Campos-Martin, J. M.; Blanco-Brieva, G.; Fierro, J. L. G. *Angew. Chem., Int. Ed.* **2006**, *45*, 6962−6984.
(8) Samanta, C. *Appl. Catal., A* **2008**, *350*, 133−149.
(9) Landon, P.; Collier, P. J.; Papworth, A. J.; Kiely, C. J.; Hutchings, G. J. *Chem. Commun.* **2002**, 2058−2059.
(10) Henkel, H.; Weber, W. U.S. Patent 1108752, 1914.
(11) Park, S.; Yoo, J.; Lee, W.; Chang, J.; Park, U.; Lee, C. U.S. Patent 5972305, 1999.
(12) Lunsford, J. H. *J. Catal.* **2003**, *216*, 455−460.
(13) Burch, R.; Ellis, P. R. *Appl. Catal., B* **2003**, *42*, 203−211.
(14) Paparatto, G.; D'Aloisio, R.; Alberti, G. D.; Furlin, P.; Arca, V.; Buzzoni, R.; Meda, L. European Patent 0978316, 1999.
(15) Zhou, B.; Lee, L. U.S. Patent 6168775, 2001.
(16) Choudhary, V. R.; Samanta, C. *J. Catal.* **2006**, *238*, 28−38.
(17) Liu, Q. S.; Lunsford, J. H. *J. Catal.* **2006**, *239*, 237−243.
(18) Edwards, J. K.; Solsona, B. E.; Landon, P.; Carley, A. F.; Herzing, A.; Kiely, C. J.; Hutchings, G. J. *J. Catal.* **2005**, *236*, 69−79.
(19) Edwards, J. K.; Solsona, B.; Ntainjua N, E.; Carley, A. F.; Herzing, A. A.; Kiely, C. J.; Hutchings, G. J. *Science* **2009**, *323*, 1037−1041.
(20) Rankin, R. B.; Greeley, J. *ACS Catal.* **2012**, *2*, 2664−2672.
(21) McIntyre, J. A. U.S. Patent 5512263, 1996.
(22) Melada, S.; Pinna, F.; Strukul, G.; Perathoner, S.; Centi, G. *J. Catal.* **2005**, *235*, 241−248.
(23) Abate, S.; Centi, G.; Perathoner, S.; Frusteri, F. *Catal. Today* **2006**, *118*, 189−197.
(24) Abate, S.; Melada, S.; Centi, G.; Perathoner, S.; Pinna, F.; Strukul, G. *Catal. Today* **2006**, *117*, 193−198.
(25) Gao, H.; Lin, Y. S.; Li, Y.; Zhang, B. *Ind. Eng. Chem. Res.* **2004**, *43*, 6920−6930.
(26) Mancera, L. A.; Behm, R. J.; Groß, A. *Phys. Chem. Chem. Phys.* **2013**, *15*, 1497−1508.
(27) Nørskov, J. K.; Rossmeisl, J.; Logadottir, A.; Lindqvist, L.; Kitchin, J. R.; Bligaard, T.; Jonsson, H. *J. Phys. Chem. B* **2004**, *108*, 17886−17892.
(28) Michaelides, A.; Hu, P. *J. Am. Chem. Soc.* **2001**, *123*, 4235−4242.
(29) Ford, D. C.; Nilekar, A. U.; Xu, Y.; Mavrikakis, M. *Surf. Sci.* **2010**, *604*, 1565.
(30) Nyberg, C.; Tengstal, C. G. *J. Chem. Phys.* **1984**, *80*, 3463−3488.
(31) Staykov, A.; Kamachi, T.; Ishihara, T.; Yoshizawa, K. *J. Phys. Chem. C* **2008**, *112*, 19501−19505.
(32) Li, J.; Staykov, A.; Ishihara, T.; Yoshizawa, K. *J. Phys. Chem. C* **2011**, *115*, 7392−7398.
(33) Ham, H. C.; Hwang, G. S.; Han, J.; Nam, S. W.; Lim, T. H. *J. Phys. Chem. C* **2009**, *113*, 12943−12945.
(34) Todorovic, R.; Meyer, R. J. *Catal. Today* **2011**, *160*, 242−248.
(35) Zea, H.; Lester, K.; Datye, A. K.; Rightor, E.; Gulotty, R.; Waterman, W.; Smith, M. *Appl. Catal., A* **2005**, *282*, 237−245.
(36) Sales, E. A.; Jove, J.; Mendes, M. J.; Bozon-Verduraz, F. *J. Catal.* **2000**, *195*, 88−95.
(37) Sheth, P. A.; Neurock, M.; Smith, C. M. *J. Phys. Chem. B* **2005**, *109*, 12449−12466.
(38) Hammer, B.; Hansen, L. B.; Nørskov, J. K. *Phys. Rev. B* **1999**, *59*, 7413−7421.
(39) Greeley, J.; Nørskov, J. K.; Mavrikakis, M. *Annu. Rev. Phys. Chem.* **2002**, *53*, 319−348.
(40) Perdew, J. P.; Wang, Y. *Phys. Rev. B* **1992**, *45*, 13244−13249.
(41) Vanderbilt, D. *Phys. Rev. B* **1990**, *41*, 7892−7895.
(42) Payne, M. C.; Teter, M. P.; Allan, D. C.; Arias, T. A.; Joannopoulos, J. D. *Rev. Mod. Phys.* **1992**, *64*, 1045−1097.
(43) Kresse, G.; Furthmuller, J. *Comput. Mater. Sci.* **1996**, *6*, 15−50.
(44) Curtarolo, S.; Morgan, D.; Ceder, G. *Calphad* **2005**, *29*, 163−211.
(45) Müller, S.; Zunger, A. *Phys. Rev. Lett.* **2001**, *87*, 165502.
(46) Neugebauer, J.; Scheffler, M. *Phys. Rev. B* **1992**, *46*, 16067−16080.
(47) Bengtsson, L. *Phys. Rev. B* **1999**, *59*, 12301−12304.
(48) Henkelman, G.; Uberuaga, B. P.; Jonsson, H. *J. Chem. Phys.* **2000**, *113*, 9901−9904.
(49) Greeley, J.; Mavrikakis, M. *Surf. Sci.* **2003**, *540*, 215−229.
(50) Schmidt, P. K.; Christmann, K.; Kresse, G.; Hafner, J.; Lischka, M.; Groß, A. *Phys. Rev. Lett.* **2001**, *87*, 096103.
(51) Kubas, G. J. *Acc. Chem. Res.* **1988**, *21*, 120−128.
(52) Khan, N. A.; Shaikhutdinov, S.; Freund, H. J. *Catal. Lett.* **2006**, *108*, 159−164.
(53) Chen, A. C.; Adams, B. D.; Ostrom, C. K.; Chen, S. A. *J. Phys. Chem. C* **2010**, *114*, 19875−19882.
(54) Xu, Y.; Greeley, J.; Mavrikakis, M. *J. Am. Chem. Soc.* **2005**, *127*, 12823−12827.

(55) Wouda, P. T.; Schmid, M.; Nieuwenhuys, B. E.; Varga, P. *Surf. Sci.* **1999**, *423*, L229−L235.
(56) Chinta, S.; Lunsford, J. H. *J. Catal.* **2004**, *225*, 249−255.
(57) Laursen, A. B.; Man, I. C.; Trinhammer, O. L.; Rossmeisl, J.; Dahl, S. *J. Chem. Educ.* **2011**, *88*, 1711−1715.
(58) Coulthard, I.; Sham, T. K. *Phys. Rev. Lett.* **1996**, *77*, 4824−4827.
(59) Mavrikakis, M.; Stoltze, P.; Nørskov, J. K. *Catal. Lett.* **2000**, *64*, 101−106.
(60) Chen, M. S.; Kumar, D.; Yi, C. W.; Goodman, D. W. *Science* **2005**, *310*, 291−293.
(61) Zhong, D. Y.; Franke, J. H.; Podiyanachari, S. K.; Blomker, T.; Zhang, H. M.; Kehr, G.; Erker, G.; Fuchs, H.; Chi, L. F. *Science* **2011**, *334*, 213−216.
(62) Wouda, P. T.; Schmid, M.; Nieuwenhuys, B. E.; Varga, P. *Surf. Sci.* **1998**, *417*, 292−300.
(63) Gonzalez, S.; Neyman, K. M.; Shaikhutdinov, S.; Freund, H. J.; Illas, F. *J. Phys. Chem. C* **2007**, *111*, 6852−6856.
(64) Shu, J.; Bongondo, B. E. W.; Grandjean, B. P. A.; Adnot, A.; Kaliaguine, S. *Surf. Sci.* **1993**, *291*, 129−138.
(65) Greeley, J.; Mavrikakis, M. *Nat. Mater.* **2004**, *3*, 810−815.
(66) Kitchin, J. R.; Reuter, K.; Scheffler, M. *Phys. Rev. B* **2008**, *77*, 075437.
(67) Svenum, I.-H.; Herron, J. A.; Mavrikakis, M.; Venvik, H. J. *Catal. Today* **2012**, *193*, 111−119.
(68) Grabow, L. C.; Gokhale, A. A.; Evans, S. T.; Dumesic, J. A.; Mavrikakis, M. *J. Phys. Chem. C* **2008**, *112*, 4608−4617.
(69) Gokhale, A. A.; Dumesic, J. A.; Mavrikakis, M. *J. Am. Chem. Soc.* **2008**, *130*, 1402−1414.
(70) Ojeda, M.; Li, A. W.; Nabar, R.; Nilekar, A. U.; Mavrikakis, M.; Iglesia, E. *J. Phys. Chem. C* **2010**, *114*, 19761−19770.
(71) Ojeda, M.; Nabar, R.; Nilekar, A. U.; Ishikawa, A.; Mavrikakis, M.; Iglesia, E. *J. Catal.* **2010**, *272*, 287−297.